THE JOURNAL OF
PHYSICAL CHEMISTRY
LETTERS
A JOURNAL OF THE AMERICAN CHEMICAL SOCIETY

Gas-Phase Synthesis of Germanium Monosulfide (GeS, $X^1\Sigma^+$) via the Elementary Reaction of Atomic Germanium (Ge, ^3P) with Hydrogen Sulfide (H_2S, X^1A_1)

Surajit Metya, Shane J. Goettl, Iakov A. Medvedkov, Márcio O. Alves, Breno R. L. Galvão,* and Ralf I. Kaiser*

Cite This: *J. Phys. Chem. Lett.* 2025, 16, 4780−4787

Read Online

ACCESS | Metrics & More | Article Recommendations | SI Supporting Information

ABSTRACT: Germanium belongs to the carbon group in the periodic table; however, its chemical behavior sometimes differs from that of carbon, defying the isoelectronic rule proposed by Langmuir. One notable example is germanium monosulfide (GeS, $X^1\Sigma^+$), where germanium exhibits remarkable stability in the +II oxidation state, unlike carbon in its monosulfide form. Germanium monosulfide (GeS, $X^1\Sigma^+$) is a promising material, with applications ranging from optoelectronic devices to highly efficient semiconductors. Here, we report on the gas phase synthesis of germanium monosulfide (GeS) through the elementary reaction between ground-state atomic germanium (Ge, ^3P) and hydrogen sulfide (H_2S, X^1A_1) via nonadiabatic reaction dynamics exploiting the single-collision approach in a crossed molecular beams machine. The integration of electronic structure calculations and experimental findings reveals that the reaction dynamics proceed via intersystem crossing (ISC) to produce singlet germanium monosulfide (GeS, $X^1\Sigma^+$) and molecular hydrogen. This result provides an intricate reaction mechanism for the germanium−hydrogen sulfide system via germanium−sulfur bond coupling and demonstrates the "heavy atom effect" facilitated intersystem crossing yielding nearly exclusive singlet germanium monosulfide. This outcome also emphasizes that elementary reactions involving atomic germanium and hydrogen sulfide are quite different from those observed in the carbon−hydrogen sulfide or silicon−hydrogen sulfide systems.

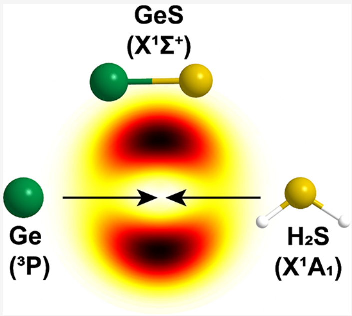

The concept of isoelectronicity has significantly influenced synthetic chemistry over the past century by explaining the reactivity of isoelectronic systems and reinforcing the principles of chemical bonding theory.[1] This concept has enriched the chemistry of silicon, germanium, and tin in recent decades, drawing significant attention and establishing parallels with the analogous carbon chemistry.[2−13] Each group 14 element has four valence electrons, allowing them to form stable compounds with four coordination. Isoelectronicity theory, however, struggles to explain the structure and properties of low-coordination compounds of the group 14 elements. Although the existence of such compounds has long been a subject of vigorous debate within the scientific community, recent advances in techniques for analyzing electronic structures and chemical bonding have confirmed their existence.[3,12−21] The dihydride of carbon, methylene (CH_2, X^3B_1), possesses a triplet ground-state with singlet−triplet energy splitting to the a^1A_1 state of 36−38 kJ mol^{-1}.[22,23] In contrast, the higher homologues, silylene (SiH_2) and germylene (GeH_2), have a singlet (X^1A_1) electronic ground-state, with singlet−triplet energy splitting of 80−88 kJ mol^{-1} and 100−105 kJ mol^{-1}, respectively.[24−29] Bond angles ($\angle_{H-M-H}$, where M = C, Si, Ge) also differ, decreasing from 129.8° in CH_2 to 93.4° in SiH_2 and 92.3° in GeH_2, attributed to increasing valence orbital size from carbon to germanium which in turn weakens the effectiveness of hybridization between the s and p orbitals.[29−31] This is also reflected in the decreasing reactivity of the dihydrides of this group from carbon to the heavier members.[8,18,32−37] A similar distinction in bonding is seen in diatomic subvalent compounds, where carbon monoxide (CO) forms a triple bond ($C\equiv O$), while silicon monoxide (SiO) and germanium monoxide (GeO) each feature a single π bond and a σ bond. This difference is reflected in the increasing bond lengths, from 1.128 Å in CO to 1.512 Å in SiO and 1.617 Å in GeO.[38] Importantly, the reaction dynamics for the synthesis of low-valent compounds of these elements in group 14 are quite different. For example, gas-phase synthesis of silicon monoxide and germanium monoxide by the reaction of atomic Si or Ge with oxygen are observed to follow a different mechanistic pathway.[12,13]

On the other hand, increasing interest in the (in)organic germanium (Ge, discovered in 1886 by Clemens Winkler[39,40])

Received: February 24, 2025
Revised: May 2, 2025
Accepted: May 2, 2025
Published: May 7, 2025

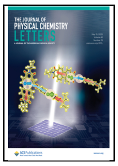

https://doi.org/10.1021/acs.jpclett.5c00574

chemistry has also revitalized extensive research on the chemical bonding in binary sulfides of group 14 elements. Germanium monosulfide (GeS) has gained attention for its anisotropic properties and layered, semiconducting nature, making it valuable for optoelectronic devices like photodetectors, solar cells, and thin-film transistors.[41−49] Additionally, GeS serves as an anode material in lithium-ion batteries and finds application in thermoelectric devices for energy conversion.[50,51] There are various reports in the literature on the synthesis of GeS in the condensed phase.[52−54] Kalebaila et al. synthesized solid GeS from Ge(IV)ethoxide ($Ge(OEt)_4$) and hydrogen sulfide (H_2S).[52] Similarly, Lee and co-workers report the synthesis using a one-pot heating method with GeI_4, 1-octadecene, oleylamine, and 1-dodecanethiol at 593 K, characterizing GeS nanosheets via X-ray diffraction, scanning electron microscopy (SEM), and transmission electron microscopy (TEM).[53]

Although GeS has been synthesized as nanoparticles or nanosheets, no direct method for preparing divalent germanium monosulfide (GeS) exists. Here, we report the first gas-phase synthesis of GeS via a single-collision event between ground-state germanium (Ge, ^3P) and hydrogen sulfide (H_2S, X^1A_1). The cross-molecular beam studies combined with electronic structure calculations offer valuable insights into the reaction dynamics involved in the formation of subvalent germanium monosulfide (GeS), providing detailed information on products, intermediates, and branching ratios.[55−57] In this approach, two highly diluted molecular beams with controlled velocities and electronic states intersect under single-collision conditions, minimizing intrabeam collisions and eliminating secondary interactions.[55−57] The reaction between germanium germanium (Ge, ^3P) and hydrogen sulfide (H_2S, X^1A_1) follows a nonadiabatic pathway via intersystem crossing (ISC) between singlet and triplet surfaces, significantly enhanced by the heavy atom effect of germanium. These findings also serve as a benchmark, providing insights into germanium−sulfur chemistry, a field that has been challenging to study until now.

For the reaction between germanium (Ge, ^3P) and hydrogen sulfide (H_2S, X^1A_1) a reactive scattering signal was recorded at the mass-to-charge ratios (m/z) from 102 to 110 considering the naturally occurring isotopes of germanium (^{70}Ge (20.4%), ^{72}Ge (27.3%), ^{73}Ge (7.7%), ^{74}Ge (36.7%), and ^{76}Ge (7.8%)) and sulfur (^{32}S (94.8%), ^{33}S (0.8%), and ^{34}S (4.4%)). The signal observed at m/z = 106 ($^{74}Ge^{32}S^+$/$^{72}Ge^{34}S^+$/$^{73}Ge^{34}SH^+$) exhibited the highest signal-to-noise ratio. However, time-of-flight (TOF) mass spectra observed for all of the lower mass-to-charge ratio signals are superimposable and hence originate from the same channel and hence chemical reaction. The data at m/z = 106 can be best fit with a reaction channel involving the elimination of molecular hydrogen (H_2, m/z = 2; reaction 1). Furthermore, it should be emphasized that all attempts to fit the experimental data with the atomic hydrogen loss (H, m/z = 1) reaction were unsuccessful. Figure 1 shows the corresponding laboratory angular distribution (LAD) and the TOF recorded at the signal of m/z = 106. TOFs were recorded at the center-of-mass angle of 8.25° and in steps of 1° (lower angles) and 2° (higher angles). The complete laboratory angular distribution was narrowly confined ranging from 16.25° beyond the detection limit of the rotating detectors at small angles of less than 6.25°. All TOF spectra were some 200 μs wide spanning a range from 290 to 490 μs. Overall, the laboratory data indicates the formation of germanium monosulfide (GeS) with the loss of molecular hydrogen in the reaction between germanium (Ge, ^3P) and hydrogen sulfide (H_2S, X^1A_1) via reaction 1.

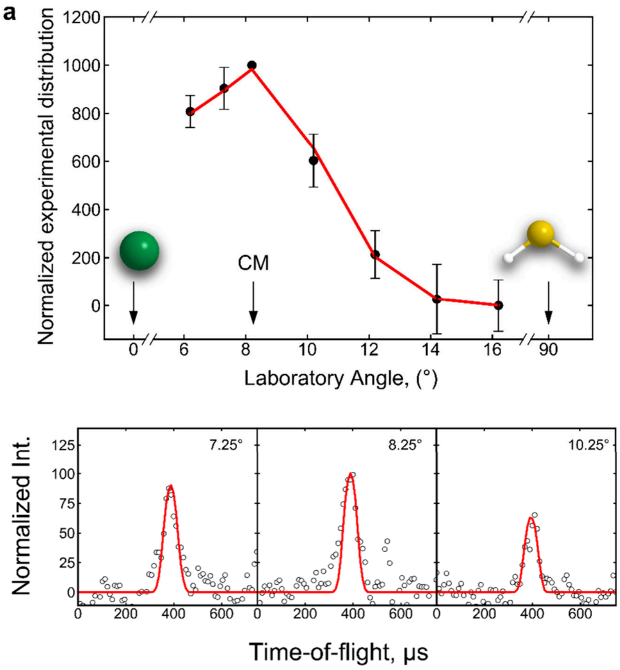

Figure 1. (a) Laboratory angular distribution and (b) time-of-flight (TOF) spectra obtained at m/z 106 for the reaction involving atomic germanium (^{74}Ge, ^3P) and hydrogen sulfide (H_2S, X^1A_1). The experimental results are represented by black circles, and the red lines illustrate the best fits.

$$^{74}\mathrm{Ge}(^3\mathrm{P}) + \mathrm{H_2}{}^{32}\mathrm{S}(\mathrm{X}^1\mathrm{A}_1) \rightarrow {}^{74}\mathrm{Ge}^{32}\mathrm{S}(\mathrm{X}^1\Sigma^+) + \mathrm{H_2}(\mathrm{X}^1\Sigma_g) \tag{1}$$

To gain deeper insights into the underlying reaction mechanisms, particularly the involvement of intersystem crossing (ISC), excited-state surfaces, and nonadiabatic reaction dynamics, the laboratory data were transformed from the laboratory reference frame to the center-of-mass (CM) reference frame. This transformation was achieved by using a forward convolution routine employing a single channel fit of the laboratory data in conjunction with reaction 1. Figure 2 presents the two "best fit" CM functions obtained from this approach: CM translational energy distribution [$P(E_T)$] and angular flux distributions [$T(\theta)$]. Crucial insights into the reaction channel and dynamics are obtained through a thorough analysis of these CM functions. The maximum translational energy release (E_{max}) was determined from the derived $P(E_T)$ distribution to be 342 ± 72 kJ mol^{-1}. According to energy conservation, this maximum translation energy released represents the sum of the collision energy (E_c) and the reaction exoergicity for the fraction of product molecules formed without internal excitation. Considering the collision energy for the reaction of 91 ± 2 kJ mol^{-1}, the reaction was determined to be exoergic by 250 ± 73 kJ mol^{-1}. However, not all the products formed after collision have the maximum kinetic energy; only those that are born without internal excitation will follow this energy conservation rule. The average translational energy of the products was determined to be 92 ± 19 kJ mol^{-1}, indicating that 27 ± 11% of the total available energy is directed into the translational degrees of freedom of the products. This observation suggests that the

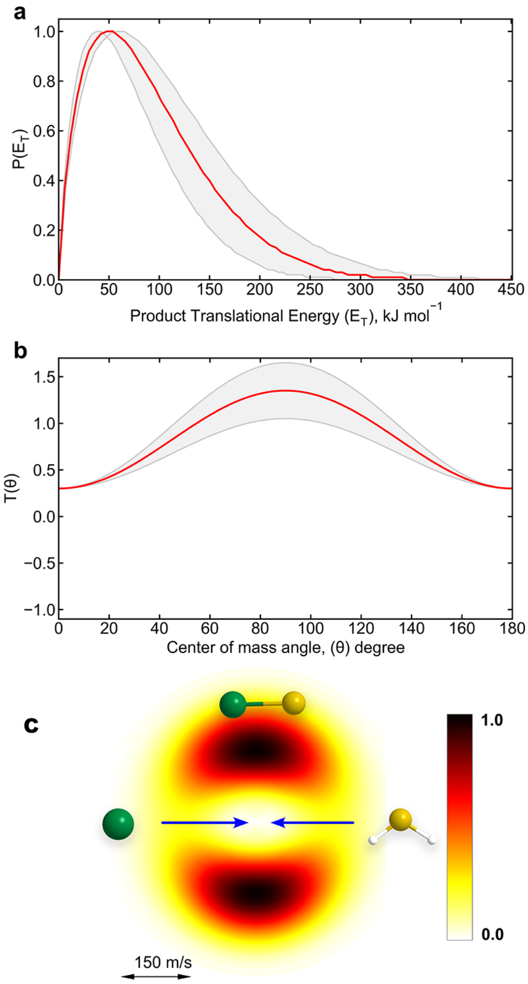

Figure 2. (a) Center-of-mass translational energy distribution $P(E_T)$, (b) angular flux distribution $T(\theta)$, and (c) flux contour map (top view) leading to the formation of germanium monosulfide (GeS, $C_{\infty v}$, $X^1\Sigma^+$) from the reaction between atomic germanium (Ge, ^3P) and hydrogen sulfide (H_2S, X^1A_1). The solid red lines indicate the best fit, while the shaded regions represent the error margins. The direction of the germanium beam is defined by 0°, while that of the hydrogen sulfide is at 180°. Atoms are color-coded in green (germanium), yellow (sulfur), and white (hydrogen).

reaction mechanism involves the formation of a covalently bound intermediate.[57] Additionally, $T(\theta)$ exhibits intensity across the entire angular range from 0° to 180°, displaying forward−backward symmetry with a peak at 90°. These findings indicate indirect scattering dynamics involving a $GeSH_2$ complex with a lifetime exceeding its rotational period, undergoing unimolecular decomposition via molecular hydrogen loss parallel to the total angular momentum vector. In a reactive scattering experiment, the total angular momentum (**J**) is the vector sum of the orbital angular momentum (**L**) and the rotational angular momentum (**j**) of the reactants, which remain unchanged and equal to the sum of the orbital (**L′**) and rotational (**j′**) angular momenta of the product, i.e., $\mathbf{J} = \mathbf{L} + \mathbf{j} = \mathbf{L}' + \mathbf{j}'$.[58] In the experimental condition, $\mathbf{J} \approx \mathbf{L}$, as rotational angular momentum (**j**) reduced significantly due to the rotational cooling in the supersonic expansion. Furthermore, if the product receives very little rotational excitation ($\mathbf{j}' \approx 0$), such that $\mathbf{L} \approx \mathbf{L}'$, and the dissociation occurs in a plane perpendicular to the relative velocity vector, the intensity appears on the side of the relative velocity vector, as also depicted in the flux contour map. The contour map illustrates the flux intensity of the reactive scattering products as a function of product velocity (u) and center-of-mass scattering angle (θ), offering detailed insights into the reactive scattering process.[59]

The underlying mechanism and the dynamics of the Ge(^3P)−H_2S (X^1A_1) reaction are now revealed by the combination of the experimental laboratory data and electronic structure calculations. Calculated potential energy surfaces (PES) (Figure 3) include four singlet intermediates (**i1**, **i2**, **i3**, **i4**), three triplet intermediates (**i5**, **i6**, **i7**), ten transition states (**TS1**−**TS10**), and one singlet−triplet seam of crossing (**MSX1**) along with the four possible products: singlet germanium monosulfide (GeS, **p1**, $C_{\infty v}$, $X^1\Sigma^+$) and triplet germanium monosulfide (GeS, **p3**, $C_{\infty v}$, $a^3\Pi$), which arose from the loss of molecular hydrogen, and germanium hydrosulfide (GeSH, **p2**, C_s, X^2A') and thiogermaniumformyl radical (HGeS, **p4**, C_s, X^2A') formed via the loss of atomic hydrogen. The reaction is initiated on a triplet surface through the barrierless addition of ground-state atomic germanium Ge(^3P) to the sulfur atom of H_2S leading to Ge−S bond formation. The resulting triplet $GeSH_2$ intermediate (**i5**, C_s, X^3A'') can react via multiple competing pathways. One possibility involves the dissociation of the S−H bond leading to the formation of doublet GeSH (**p2**, C_s, X^2A') and atomic hydrogen; this pathway requires overcoming an energy barrier of 61 kJ mol^{-1} above the separated reactants. Alternatively, **i5** can undergo hydrogen migration from the sulfur atom to the germanium atom forming the triplet intermediate λ^2-germainthiol (HGeSH, **i6**, C_1, a^3A) via a barrier of 44 kJ mol^{-1}. The triplet intermediate **i6** can eliminate atomic hydrogen from the sulfur atom resulting in the formation of thiogermaniumformyl radical (HGeS, **p4**, C_s, X^2A') and atomic hydrogen, with an exit barrier of 86 kJ mol^{-1} above the separated reactants. Another pathway involves the simultaneous breaking of the S−H and Ge−H bonds accompanied by molecular hydrogen formation, leading to the formation of triplet germanium monosulfide (GeS, **p3**, $C_{\infty v}$, $a^3\Pi$). Additionally, intermediate **i6** can undergo yet another hydrogen migration from the sulfur to the germanium atom, forming the germanethione intermediate (H_2GeS, **i7**, C_s, a^3A''). This intermediate can then produce thiogermaniumformyl radical (HGeS, **p4**, C_s, X^2A') through the barrierless elimination of one hydrogen atom. Overall, three reaction products **p2** to **p4** can be accessed on the triplet surface via atomic (**p2**, **p4**) and molecular hydrogen loss (**p3**).

How can the singlet surface be accessed? Electronic structure calculations reveal that an electronically excited germanium atom Ge(^1D) can add to the sulfur atom of H_2S forming the singlet $GeSH_2$ complex (**i1**, C_s, a^1A'). This intermediate undergoes hydrogen migration from the sulfur atom to the germanium atom yielding the singlet λ^2-germainthiol intermediate (HGeSH, **i2**, C_s, X^1A'). Commencing with **i2**, hydrogen elimination from either the Ge or S atom leads to germanium hydrosulfide (GeSH, **p2**, C_s, X^2A') or thiogermaniumformyl radical (HGeS, **p4**, C_s, X^2A'), respectively. Intermediate **i2** can also facilitate molecular hydrogen elimination producing singlet germanium monosulfide (GeS, **p1**, $C_{\infty v}$, $X^1\Sigma^+$). Alternatively, **i2** may undergo isomerization via Ge−S bond rotation to trans-λ^2-germainthiol (HGeSH, **i3**, C_s, X^1A') with a barrier of 53 kJ mol^{-1}, followed by hydrogen migration from the sulfur to germanium atom forming germanethione (H_2GeS, **i4**, C_{2v}, X^1A_1). Intermediate **i4** can

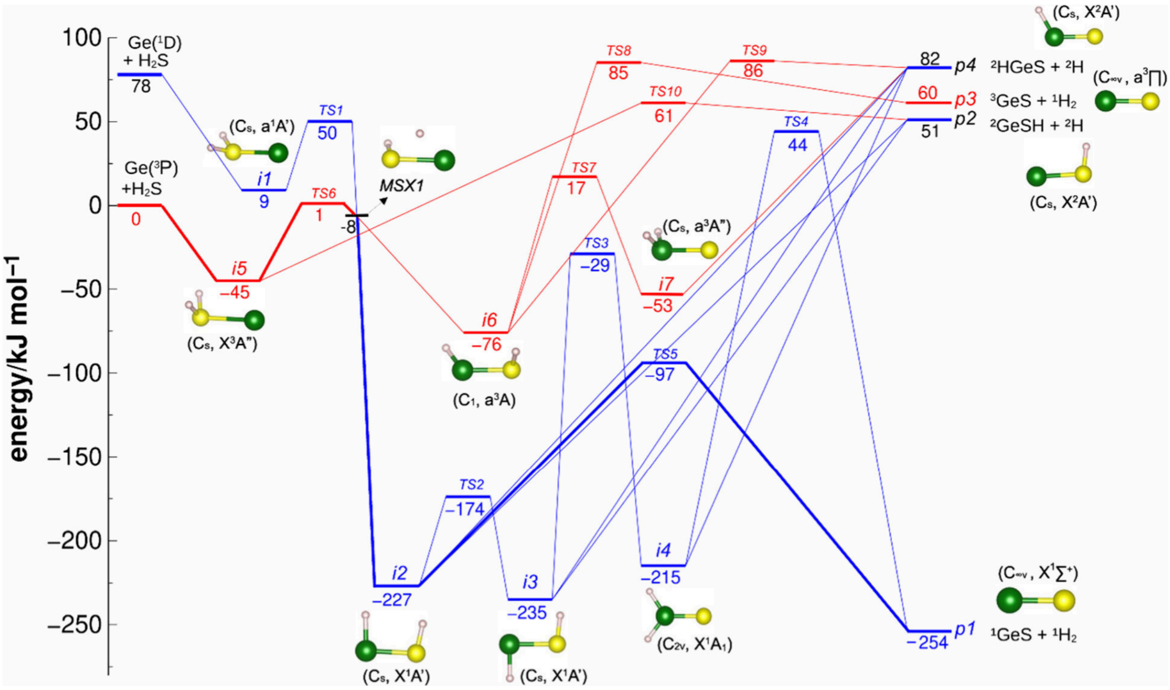

Figure 3. Potential energy surface of the reaction of atomic germanium (Ge, ^3P) and hydrogen sulfide (H_2S, X^1A_1). Red lines represent the triplet surface, while blue lines indicate the singlet surface. The numbers denote energies (in kJ mol^{-1}) for each species calculated at the CCSD(T)-F12/aug-cc-pVQZ//M06-2X/cc-pVTZ+ZPE(M06-2X/cc-pVTZ) level of theory. Point groups and electronic states are provided in parentheses. Atoms are color-coded in green (germanium), yellow (sulfur), and white (hydrogen). The most favorable path for this reaction is highlighted in bold lines.

then dissociate into singlet germanium monosulfide (GeS, **p1**, $C_{\infty v}$, and $X^1\Sigma^+$) and molecular hydrogen (H_2, $D_{\infty h}$, and $X^1\Sigma_g$).

In order to appraise the possibility of the intersystem crossing (ISC) from the triplet to the singlet surface, calculations were also extended in search of the minima on the seam of crossing. This investigation also identified one minimum on the seam of crossing (**MSX1**) located in the vicinity of the transition states for the hydrogen migration from sulfur to the germanium atom connecting the intermediates **i5** and **i6**. **MSX1**, residing 8 kJ mol^{-1} below the separate reactants, is connecting the triplet intermediate **i5** with the singlet intermediate **i2** by the ISC with a spin−orbit coupling (SOC) of 382 cm^{-1}. The spin−orbit coupling (SOC) is significantly higher in the reaction between atomic germanium (Ge, ^3P) and H_2S compared to similar systems involving atomic silicon (Si, ^3P)[60] of 71 cm^{-1}, making it the crucial step in this reaction.

The computed reaction energy for the formation of singlet germanium monosulfide (GeS, **p1**, $C_{\infty v}$, $X^1\Sigma^+$) and molecular hydrogen (H_2, $D_{\infty h}$, $X^1\Sigma_g$) is −254 kJ mol^{-1}. For the reaction channels **p2**, **p3**, and **p4**, the computed reaction energies are +51, +60, and +82 kJ mol^{-1}, respectively. The experimentally determined reaction energy (−250 ± 73 kJ mol^{-1}) for the molecular hydrogen loss channel supports the formation of the most thermodynamically stable product ground-state singlet germanium monosulfide (GeS, **p1**, $C_{\infty v}$, $X^1\Sigma^+$) via molecular hydrogen (H_2, $D_{\infty h}$, $X^1\Sigma_g$) loss. The previously reported LIF characterization of the Ge atom in a molecular beam indicates the presence of Ge($^3P_0$), Ge($^3P_1$), and Ge($^3P_2$) states.[11] Compared with Ge($^3P_0$), the Ge($^3P_1$) and Ge($^3P_2$) states are higher in energy by 6.7 and 16.9 kJ mol^{-1}, respectively. While these energy differences could slightly alter the reaction energy, they remain within the margin of our experimental error.

Combining experimental results with electronic structure calculations for the reaction between ground-state germanium atom (Ge, ^3P) and hydrogen sulfide (H_2S, X^1A_1), singlet germanium monosulfide (GeS, **p1**, $C_{\infty v}$, $X^1\Sigma^+$) emerges as the most likely product, resulting from the loss of molecular hydrogen (H_2, $D_{\infty h}$, $X^1\Sigma_g$). While calculations reveal multiple mechanistic pathways for product formation, the experimentally derived $P(E_T)$ and $T(\theta)$ serve as constraints to identify the most favorable routes. The peak at 51 ± 11 kJ mol^{-1} in the experimentally determined $P(E_T)$ indicates a tight exit transition state for product formation. On the other hand, the reaction initiated on the triplet surface lacks an adiabatic pathway leading to the formation of singlet germanium monosulfide (GeS, **p1**, $C_{\infty v}$, $X^1\Sigma^+$). This indicates that the mechanistic pathway must involve a nonadiabatic transition via intersystem crossing (ISC) from the triplet to the singlet surface. In this case, the reaction starts with the formation of the intermediate $GeSH_2$ (**i5**, C_s, X^3A'') formed via barrierless addition of atomic germanium to the sulfur atom of hydrogen sulfide. Then it follows the pathway from intermediate **i5** to intermediate **i2** via intersystem crossing at **MSX1**. At this point, it is important to mention that the "heavy atom effect" of germanium likely plays a major role in intersystem crossing (ISC) during the reaction due to the spin−orbit coupling resulting from significant relativistic effects.[61−64] Considering the high spin−orbit coupling ISC from **i5** to **i2** through **MSX1**, this pathway represents the key step in this reaction. Starting from the intermediate **i2**, two favorable pathways culminate in the formation of the most stable singlet germanium monosulfide (GeS, **p1**, $C_{\infty v}$, $X^1\Sigma^+$) which proceeds either via **i2** → **TS5** → **p1** (path **A**) or via **i2** → **TS2** → **i3** → **TS3** → **i4** → **TS4** → **p1** (path **B**). The computed geometry of **TS5**, the exit transition states for path **A** (Figure 4b), shows that a molecular hydrogen loss is almost parallel (∼11°) to the total

https://doi.org/10.1021/acs.jpclett.5c00574
J. Phys. Chem. Lett. 2025, 16, 4780−4787

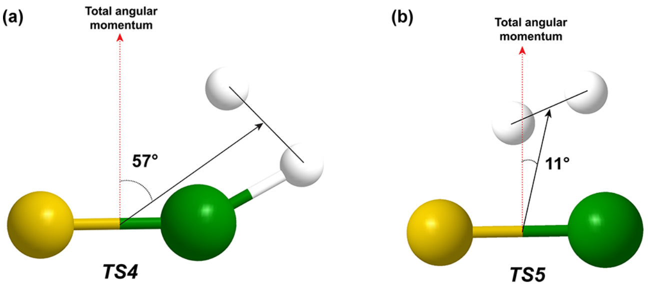

Figure 4. Computed geometries of the exit transition state, (a) **TS4** and (b) **TS5**, lead to the formation of germanium monosulfide (GeS, **p1**, $C_{\infty v}$, $X^1\Sigma^+$). Atoms are color-coded in green (germanium), yellow (sulfur), and white (hydrogen). The red dotted arrow represents the direction of the total angular momentum vector perpendicular to the relative velocity vector. The black arrow represents the direction of the dissociation of the H_2.

angular momentum vector. This satisfies the prediction of geometrical constraints made from the experimentally derived angular flux distribution [$T(\theta)$]. On the other hand, the geometry of **TS4**, the exit transition state for path **B** (Figure 4a), depicts the elimination of molecular hydrogen making an angle of about 57°. This result demonstrates that the experimentally observed most favorable pathway is path **A** leading to the formation of singlet germanium monosulfide (GeS, **p1**, $C_{\infty v}$, and $X^1\Sigma^+$). Additionally, we derived energy-dependent rate constants and the statistical branching ratio for these two competing paths using RRKM theory, considering the **i2** intermediate as the starting point and **p1** as the end point connecting paths **A** or **B**. The results indicate that, if the system behaves statistically, the ratio of reaction fluxes between the two pathways (**A** and **B**) at the experimental collision energy of 91 ± 2 kJ mol^{-1} should be approximately 99:1.

In summary, our crossed molecular beam experiment combined with the electronic structure and statistical calculation unveil the mechanistic pathway of the formation of singlet germanium monosulfide (GeS, **p1**, $C_{\infty v}$, $X^1\Sigma^+$) from the elementary gas phase reaction between ground-state germanium atom (Ge, ^3P) and hydrogen sulfide (H_2S, X^1A_1) involving nonadiabatic reaction dynamics of long-lived $GeSH_2$ intermediate. The reaction begins on the triplet surface with a barrierless addition of the germanium atom (Ge, ^3P) and H_2S, leading to the $GeSH_2$ intermediate (**i5**, C_s, X^3A'') by the formation of a Ge−S covalent bond. This $GeSH_2$ intermediate then proceeds through a nonadiabatic triplet to singlet intersystem crossing (ISC) to form singlet λ^2-germainthiol intermediate (HGeSH, **i2**, C_s, X^1A') via hydrogen migration from sulfur to germanium atom. Intersystem crossing plays the key role in this reaction because of the high spin−orbit coupling due to the "heavy atom effect" of the germanium. Ultimately this leads to the formation of singlet germanium monosulfide (GeS, **p1**, $C_{\infty v}$, $X^1\Sigma^+$) overcoming a tight exit barrier of 130 kJ mol^{-1} with the dissociation of molecular hydrogen (H_2, $D_{\infty h}$, $X^1\Sigma_g$) in the parallel direction to the total angular momentum vector, which is perpendicular to the rotational plane. An alternative pathway for the formation of germanium monoxide (GeS, **p1**, $C_{\infty v}$, $X^1\Sigma^+$) originates from the singlet λ^2-germainthiol intermediate (HGeSH, **i2**, C_s, X^1A'), which first undergoes isomerization to trans-λ^2-germainthiol (HGeSH, **i3**, C_s, X^1A'), followed by hydrogen migration to the germanium atom, leading to the formation of germanethione (H_2GeS, **i4**, C_{2V}, X^1A_1), and finally resulting in the dissociation of molecular hydrogen to yield germanium monoxide (GeS, **p1**, $C_{\infty v}$, $X^1\Sigma^+$). However, from the RRKM calculations, it was observed that the first pathway is predominant, with a branching ratio of approximately 99:1. This study clarifies the basic differences in reaction mechanisms involved in the formation of monosulfide of group 14 through an atom-neutral type of reaction emphasizing the creation of subvalent germanium(II) compounds such as germanium monosulfide (GeS, $C_{\infty v}$, $X^1\Sigma^+$).

■ MATERIALS AND METHODS

The gas-phase reaction between the ground-state germanium atom (Ge, ^3P) and hydrogen sulfide (H_2S, X^1A_1) under single-collision conditions has been studied using a cross-molecular beam setup.[65,66] Details of the experimental procedure and the data processing methods are described in the Supporting Information. A supersonic beam of atomic germanium was generated through laser ablation by using the 266 nm output of a Nd:YAG laser (6 mJ, 30 Hz; Quanta-Ray) focused at a rotating Ge rod (99.98%, Alfa Aesar). The resulting Ge atoms were seeded into a pulsed supersonic helium (He, 99.9999%, Matheson) beam, produced by a 60 Hz Porch-Trickl pulsed valve with a backing pressure of 4 atm. The beam was first skimmed and then chopped to select a particular velocity with a four-slot chopper wheel. The peak velocity (v_p) was measured at 2683 ± 26 m s^{-1}, and the speed ratio (S) of the beam was determined to be 2.5 ± 0.2. The supersonic beam of hydrogen sulfide crossed the primary atomic beam perpendicularly; the hydrogen sulfide beam was characterized via v_p = 805 ± 9 m s^{-1} and S = 14.4 ± 0.1 and prepared utilizing also a 60 Hz Proch-Trickl pulse valve with a backing pressure of 550 Torr. Both of the pulse valves are operated at −400 V with a pulse width of 80 μs. Reactant species from two supersonic beams collide with each other in the scattering chamber at a mean collision energy of E_c = 91 ± 2 kJ mol^{-1}. Reactively scattering products were detected by a rotatable, triply differentially pumped mass spectrometric detector. Products were first ionized at the entrance of the detector with 80 eV electrons at an emission current of 2 mA by a Brink-type electron ionizer. Subsequent ions are filtered according to m/z by a quadrupole mass spectrometer (QMS, Extrel, QPS, 1.2 MHz) and detected with a Daly type particle ion counter.[67] Time-of-flight mass spectra were taken between 6.25° and 16.25° in steps of two degrees with respect to the primary atomic germanium beam. To ensure accurate data collection during TOF recording, instant background subtraction was implemented by running the laser at half of the pulse valve operating frequency.

The laboratory angular distribution (LAD) and time-of-flight (TOF) spectra were then transformed from the laboratory frame to the center-of-mass frame through a forward convolution procedure to analyze the reaction dynamics.[68,69] In this process, user-defined angular flux $T(\theta)$ and translation energy distribution $P(E_T)$ in the center-of-mass (CM) frame were used to simulate time-of-flight (TOF) spectra and the laboratory angular distribution (LAD). These parameters were iteratively refined until the best fit for both the TOFs and LAD was achieved. These center-of-mass (CM) functions collectively form a differential reactive cross-section $I(u,\theta) \approx P(u) \times T(\theta)$ representing intensity as a function of angle θ and velocity u in the CM frame, which can be visualized using a contour map.

https://doi.org/10.1021/acs.jpclett.5c00574
J. Phys. Chem. Lett. 2025, 16, 4780−4787

The quantum chemical calculations reported in this work were carried out using the GAMESS-US[70] and MOLPRO[71] packages. We have performed geometry optimizations using density functional theory[72] (DFT) employing the M06-2X[73] exchange and correlation functional with the cc-pVTZ basis set.[74,75] This functional was chosen due to its superior performance on barrier heights (both hydrogen-transfer and non-hydrogen-transfer), with mean errors of about 5 kJ mol^{-1}.[76] At the optimized structures of the intermediate and transition states, we calculate the Hessian matrix to obtain vibrational frequencies and zero-point energy (ZPE) corrections. We have determined the minimum on the seam of crossing (MSX) between singlet and triplet electronic PESs at this level of theory by performing an optimization with a Lagrange multiplier to constrain equal energy on the two states. However, vibrational frequencies and ZPE corrections for MSXs cannot be obtained similarly to intermediates and transition states, as such structures are not conventional stationary structures on the PES. For this, we first calculate the Hessian matrix for each state independently of the MSX geometry. The coordinate perpendicular to the seam is then projected out (with the rotational and translational degrees of freedom) to yield an effective Hessian matrix, as described in refs 77−79. This matrix is finally diagonalized to provide the $3N - 7$ vibrational frequencies of the MSX, using the implementation described by Gannon et al.[80] The ZPE corrections for the MSX are then obtained from these frequencies.

To improve the accuracy of our results, at each structure optimized at the M06-2X/cc-pVTZ level we calculate single point energies with the explicitly correlated coupled cluster method with single, doubles plus perturbative triples excitations[81,82] (CCSD(T)-F12) method and with the aug-cc-pVQZ basis set. The overall approach is then abbreviated as CCSD(T)-F12/aug-cc-pVQZ//M06-2X/cc-pVTZ+ZPE-(M06-2X/cc-pVTZ). From previous and extensive benchmarks, this methodology shows an accuracy within 4 kJ mol^{-1}.[83]

The chance of a triplet−singlet transition depends on the magnitude of the spin−orbit coupling (SOC), and to predict this value, we have employed the full valence complete active space self-consistent field (CASSCF) method with the aug-cc-pVTZ basis set. The full spin−orbit matrix was calculated with the Breit−Pauli operator.[84] The spin-free electronic Hamiltonian eigenstates, $|S\rangle$, $|T, 1\rangle$, $|T, 0\rangle$, and $|T, -1\rangle$, are used to build the total Hamiltonian matrix representation ($H_{\mathrm{el}} + H_{\mathrm{SO}}$). From the matrix elements, we calculate the magnitude of the spin−orbit coupling (V_{SO}) as

$$V_{\mathrm{SO}}^{2} = \sum_{M_s=-1}^{1} \langle T, M_s|H_{\mathrm{SO}}|S\rangle^{2}$$

■ ASSOCIATED CONTENT

Supporting Information

The Supporting Information is available free of charge at https://pubs.acs.org/doi/10.1021/acs.jpclett.5c00574.

> Summary of experimentally determined velocities for each reactant (Table S1), optimized structures (Figure S1 and Figure S2), calculated harmonic frequency (Table S2), and optimized Cartesian coordinates (Table S2) for each species produced in the Ge(^{3}P)−H$_2$S(X^{1}A$_1$) system (PDF)

■ AUTHOR INFORMATION

Corresponding Authors

Breno R. L. Galvão − *Centro Federal de Educação Tecnológica de Minas Gerais, Belo Horizonte 30421-169, Brazil*; Email: brenogalvao@gmail.com

Ralf I. Kaiser − *Department of Chemistry, University of Hawai'i at Manoa, Honolulu, Hawaii 96822, United States*; orcid.org/0000-0002-7233-7206; Email: ralfk@hawaii.edu

Authors

Surajit Metya − *Department of Chemistry, University of Hawai'i at Manoa, Honolulu, Hawaii 96822, United States*; orcid.org/0009-0004-5583-8481

Shane J. Goettl − *Department of Chemistry, University of Hawai'i at Manoa, Honolulu, Hawaii 96822, United States*; orcid.org/0000-0003-1796-5725

Iakov A. Medvedkov − *Department of Chemistry, University of Hawai'i at Manoa, Honolulu, Hawaii 96822, United States*; orcid.org/0000-0003-0672-2090

Márcio O. Alves − *Centro Federal de Educação Tecnológica de Minas Gerais, Belo Horizonte 30421-169, Brazil*

Complete contact information is available at: https://pubs.acs.org/10.1021/acs.jpclett.5c00574

Notes

The authors declare no competing financial interest.

■ ACKNOWLEDGMENTS

The experimental work at the University of Hawai'i at Manoa was supported by National Science Foundation (NSF) Grant CHE 2244717. MOA and BRLG thank Conselho Nacional de Desenvolvimento Científico e Tecnológico (CNPq), grant nos. 311508/2021-9 and 405524/2021-8.

■ REFERENCES

(1) Langmuir, I. The arrangement of electrons in atoms and molecules. *J. Am. Chem, Soc.* **1919**, *41*, 868−934.

(2) Harris, D. H.; Lappert, M. F. Monomeric, volatile bivalent amides of group IV B elements, M (NR^{12})$_2$ and M (NR^{1}R^2)$_2$ (M = Ge, Sn, or Pb; R^1 = Me$_3$Si, R^2=Me$_3$C). *J. Chem. Soc., Chem. Commun.* **1974**, *21*, 895−896.

(3) Gynane, M. J.; Harris, D. H.; Lappert, M. F.; Power, P. P.; Rivière, P.; Rivière-Baudet, M. Subvalent Group 4B metal alkyls and amides. Part 5. The synthesis and physical properties of thermally stable amides of germanium (II), tin (II), and lead (II). *J. Chem. Soc., Dalton Trans.* **1977**, *20*, 2004−2009.

(4) Lischka, H.; Koehler, H. J. Ab initio investigation on the lowest singlet and triplet state of disilyne (Si$_2$H$_2$). *J. Am. Chem, Soc.* **1983**, *105*, 6646−6649.

(5) Binkley, J. Theoretical study of the relative stabilities of C2H2 and Si2H2 conformers. *J. Am. Chem, Soc.* **1984**, *106*, 603−609.

(6) Luke, B. T.; Pople, J.; Krogh-Jespersen, M.; Apeloig, Y.; Karni, M.; Chandrasekhar, J.; Schleyer, P. v. R. A theoretical survey of unsaturated or multiply bonded and divalent silicon compounds. Comparison with carbon analogs. *J. Am. Chem, Soc.* **1986**, *108*, 270−284.

(7) Palágyi, Z.; Schaefer, H. F., III; Kapuy, E. Ge2H2: a germanium-containing molecule with a low-lying monobridged equilibrium geometry. *J. Am. Chem, Soc.* **1993**, *115*, 6901−6903.

(8) Barrau, J.; Rima, G. Stable germanium analogs of carbenes, imines, ketones, thiones, selones and tellones. *Coord. Chem. Rev.* **1998**, *178*, 593−622.

(9) Wang, Y.; Xie, Y.; Wei, P.; King, R. B.; Schaefer, H. F.; von R. Schleyer, P.; Robinson, G. H. A stable silicon (0) compound with a Si= Si double bond. *Science* **2008**, *321*, 1069−1071.

(10) Nagendran, S.; Roesky, H. W. The chemistry of aluminum (I), silicon (II), and germanium (II). *Organometallics* **2008**, *27*, 457−492.

(11) Thomas, A. M.; Dangi, B. B.; Yang, T.; Tarczay, G. r.; Kaiser, R. I.; Sun, B.-J.; Chen, S.-Y.; Chang, A. H.; Nguyen, T. L.; Stanton, J. F. Directed Gas-Phase Formation of the Germaniumsilylene Butterfly Molecule (Ge (μ-H2) Si). *J. Phys. Chem. Lett.* **2019**, *10*, 1264−1271.

(12) He, C.; Goettl, S. J.; Yang, Z.; Kaiser, R. I.; Nikolayev, A. A.; Azyazov, V. N.; Mebel, A. M. Gas-Phase Preparation of Subvalent Germanium Monoxide (GeO, $X^1\Sigma^+$) via Non-Adiabatic Reaction Dynamics in the Exit Channel. *J. Phys. Chem. Lett.* **2022**, *13*, 4589−4597.

(13) He, C.; Luo, Y.; Doddipatla, S.; Yang, Z.; Millar, T. J.; Sun, R.; Kaiser, R. I. Gas-phase formation of silicon monoxide via non-adiabatic reaction dynamics and its role as a building block of interstellar silicates. *Phys. Chem. Chem. Phys.* **2022**, *24*, 19761−19772.

(14) Satgé, J.; Massol, M.; Rivière, P. Divalent germanium species as starting materials and intermediates in organo germanium chemistry. *Journal of Organometallic Chemistry* **1973**, *56*, 1−39.

(15) Petz, W. Transition-metal complexes with derivatives of divalent silicon, germanium, tin, and lead as ligands. *Chem. Rev.* **1986**, *86*, 1019−1047.

(16) Lappert, M. F.; Rowe, R. S. The role of group 14 element carbene analogues in transition metal chemistry. *Coord. Chem. Rev.* **1990**, *100*, 267−292.

(17) Neumann, W. P. Germylenes and stannylenes. *Chem. Rev.* **1991**, *91*, 311−334.

(18) Barrau, J.; Escudie, J.; Satge, J. Multiply bonded germanium species. Recent developments. *Chem. Rev.* **1990**, *90*, 283−319.

(19) Pineda, L. W.; Jancik, V.; Starke, K.; Oswald, R. B.; Roesky, H. W. Stable monomeric germanium (II) and tin (II) compounds with terminal hydrides. *Angew. Chem., Int. Ed.* **2006**, *45*, 2602−2605.

(20) Meller, A.; Pfeiffer, J.; Noltemeyer, M. Aza-und Thia-2-germa (II)-Indane und entsprechende 2, 2′-Spirobi (2-germaindane). *Z. Anorg. Allg. Chem.* **1989**, *572*, 145−150.

(21) Meller, A.; Gräbe, C. P. Synthese und Isolierung neuer Germanium (II)-Verbindungen und freier Germylene. *Chem. Ber.* **1985**, *118*, 2020−2029.

(22) McKellar, A.; Bunker, P.; Sears, T. J.; Evenson, K.; Saykally, R. J.; Langhoff, S. Far infrared laser magnetic resonance of singlet methylene: Singlet−triplet perturbations, singlet−triplet transitions, and the singlet−triplet splittinga. *J. Chem. Phys.* **1983**, *79*, 5251−5264.

(23) Leopold, D. G.; Murray, K. K.; Miller, A. E. S.; Lineberger, W. Methylene: A study of the $\tilde{X}\ {}^3B_1$ and $\tilde{a}\ {}^1A_1$ states by photoelectron spectroscopy of CH_2 and CD_2. *J. Chem. Phys.* **1985**, *83*, 4849−4865.

(24) Colvin, M. E.; Grev, R. S.; Schaefer, H. F., III; Bicerano, J. $\tilde{X}$ 1A1, $\tilde{a}$ 3B1, and $\tilde{A}$ 1B1 electronic state of silylenes. Structures and vibrational frequencies of SiH2, and SiHF, and SiF2. *Chem. Phys. Lett.* **1983**, *99*, 399−405.

(25) Rice, J.; Handy, N. The low-lying states of silylene. *Chem. Phys. Lett.* **1984**, *107*, 365−374.

(26) Gordon, M. S. Potential-energy surfaces in singlet and triplet silylene. *Chem. Phys. Lett.* **1985**, *114*, 348−352.

(27) Balasubramanian, K.; McLean, A. The singlet−triplet energy separation in silylene. *J. Chem. Phys.* **1986**, *85*, 5117−5119.

(28) Matsunaga, N.; Koseki, S.; Gordon, M. S. Relativistic potential energy surfaces of XH_2 (X= C, Si, Ge, Sn, and Pb) molecules: Coupling of ${}^1A_1$ and ${}^3B_1$ states. *J. Chem. Phys.* **1996**, *104*, 7988−7996.

(29) Mineva, T.; Russo, N.; Sicilia, E.; Toscano, M. Spectroscopic constants of SiH_2, GeH_2, SnH_2, and their cations and anions from density functional computations. *Int. J. Quantum Chem.* **1995**, *56*, 669−675.

(30) Bundhun, A.; Ramasami, P.; Schaefer, H. F., III. Germylene Energetics: Electron Affinities and Singlet−Triplet Gaps of GeX_2 and GeXY Species (X, Y = H, CH_3, SiH_3, GeH_3, F, Cl, Br, I). *J. Phys. Chem. A* **2009**, *113*, 8080−8090.

(31) Gaspar, P. P.; Xiao, M.; Pae, D. H.; Berger, D. J.; Haile, T.; Chen, T.; Lei, D.; Winchester, W. R.; Jiang, P. The quest for triplet ground state silylenes. *J. Organomet. Chem.* **2002**, *646*, 68−79.

(32) Regitz, M. Stable Carbenes—Illusion or Reality? *Angew. Chem., Int. Ed.* **1991**, *30*, 674−676.

(33) Arduengo, A. J., III; Harlow, R. L.; Kline, M. A stable crystalline carbene. *J. Am. Chem, Soc.* **1991**, *113*, 361−363.

(34) Bourissou, D.; Guerret, O.; Gabbaï, F. P.; Bertrand, G. Stable carbenes. *Chem. Rev.* **2000**, *100*, 39−92.

(35) Weidenbruch, M. Some silicon, germanium, tin, and lead analogues of carbenes, alkenes, and dienes. *Eur. J. Inorg. Chem.* **1999**, *1999*, 373−381.

(36) Gehrhus, B.; Lappert, M. F. Chemistry of thermally stable bis (amino) silylenes. *J. Organomet. Chem.* **2001**, *617*, 209−223.

(37) Kira, M. Isolable silylene, disilenes, trisilaallene, and related compounds. *J. Organomet. Chem.* **2004**, *689*, 4475−4488.

(38) Huber, K.; Herzberg, G. *Library of Congress Cataloging in Publication Data-Molecular spectra and molecular structure*; Van Nostrand Reinhold Ltd.: New York, 1979.

(39) Winkler, C. Mittheilungen über das Germanium. *J. Prakt. Chem.* **1886**, *34*, 177−229.

(40) Winkler, C. Germanium, Ge, ein neues, nichtmetallisches Element. *Ber. Dtsch. Chem. Ges.* **1886**, *19*, 210−211.

(41) Zawadzka, N.; Kipczak, Ł.; Woźniak, T.; Olkowska-Pucko, K.; Grzeszczyk, M.; Babiński, A.; Molas, M. R. Anisotropic Optical and Vibrational Properties of GeS. *Nanomaterials* **2021**, *11*, 3109.

(42) Chen, Z.; Hwang, W.; Cho, M.; Hoang, A. T.; Kim, M.; Kim, D.; Kim, D. H.; Kim, Y. D.; Kim, H. J.; Ahn, J.-H.; et al. In-plane optical and electrical anisotropy in low-symmetry layered GeS microribbons. *NPG Asia Materials* **2022**, *14*, 41.

(43) Tan, D.; Lim, H. E.; Wang, F.; Mohamed, N. B.; Mouri, S.; Zhang, W.; Miyauchi, Y.; Ohfuchi, M.; Matsuda, K. Anisotropic optical and electronic properties of two-dimensional layered germanium sulfide. *Nano Research* **2017**, *10*, 546−555.

(44) Bhatia, K.; Katyal, S. Structure and photoelectric behavior of amorphous semiconductors in the system PbS GeS GeS2. *J. Non-Cryst. Solids* **1982**, *50*, 39−48.

(45) Li, Z.; Yang, Y.; Wang, X.; Shi, W.; Xue, D.-J.; Hu, J.-S. Three-dimensional optical anisotropy of low-symmetry layered GeS. *ACS Appl. Mater. Interfaces.* **2019**, *11*, 24247−24253.

(46) Feng, M.; Liu, S.-C.; Hu, L.; Wu, J.; Liu, X.; Xue, D.-J.; Hu, J.-S.; Wan, L.-J. Interfacial Strain Engineering in Wide-Bandgap GeS Thin Films for Photovoltaics. *J. Am. Chem, Soc.* **2021**, *143*, 9664−9671.

(47) Hsueh, H. C.; Li, J. X.; Ho, C. H. Polarization photoelectric conversion in layered GeS. *Adv. Opt. Mater.* **2018**, *6*, No. 1701194.

(48) Ribeiro, T. C. Science and technology of solar cells based on SnS, SnS2 and GeS. Ph.D. Dissertation, Universidade Federal de Minas Gerais, 2023.

(49) Antunez, P. D.; Buckley, J. J.; Brutchey, R. L. Tin and germanium monochalcogenide IV−VI semiconductor nanocrystals for use in solar cells. *Nanoscale* **2011**, *3*, 2399−2411.

(50) Wei, Y.; He, J.; Zhang, Q.; Liu, C.; Wang, A.; Li, H.; Zhai, T. Synthesis and investigation of layered GeS as a promising large capacity anode with low voltage and high efficiency in full-cell Li-ion batteries. *Mater. Chem. Front.* **2017**, *1*, 1607−1614.

(51) Wang, B.; Du, W.; Yang, Y.; Zhang, Y.; Zhang, Q.; Rui, X.; Geng, H.; Li, C. C. Two-Dimensional Germanium Sulfide Nanosheets as an Ultra-Stable and High Capacity Anode for Lithium Ion Batteries. *Chem. - Eur. J.* **2020**, *26*, 6554−6560.

(52) Kalebaila, K. K.; Georgiev, D. G.; Brock, S. L. Synthesis and characterization of germanium sulfide aerogels. *J. Non-Cryst. Solids* **2006**, *352*, 232−240.

(53) Ramasamy, P.; Kwak, D.; Lim, D.-H.; Ra, H.-S.; Lee, J.-S. Solution synthesis of GeS and GeSe nanosheets for high-sensitivity photodetectors. *J. Mater. Chem. C* **2016**, *4*, 479−485.

(54) Prajapati, N.; Patel, P.; Desai, H.; Dhimmar, J.; Modi, B. Synthesis, characterization, and performance evaluation of GeS

nanoparticles in photocatalysis and sensing applications. *Appl. Phys. A: Mater. Sci. Process.* **2024**, *130*, 332.

(55) Lee, Y. T. Molecular beam studies of elementary chemical processes (Nobel lecture). *Angew. Chem., Int. Ed.* **1987**, *26*, 939−951.

(56) Gu, X.; Kaiser, R. I. Reaction Dynamics of Phenyl Radicals in Extreme Environments: A Crossed Molecular Beam Study. *Acc. Chem. Res.* **2009**, *42*, 290−302.

(57) Kaiser, R. I. Experimental investigation on the formation of carbon-bearing molecules in the interstellar medium via neutral−neutral reactions. *Chem. Rev.* **2002**, *102*, 1309−1358.

(58) Miller, W.; Safron, S.; Herschbach, D. Exchange reactions of alkali atoms with alkali halides: A collision complex mechanism. *Discuss. Faraday Soc.* **1967**, *44*, 108−122.

(59) Levine, R. D. *Molecular reaction dynamics*; Cambridge University Press: 2009.

(60) Doddipatla, S.; He, C.; Goettl, S. J.; Kaiser, R. I.; Galvão, B. R.; Millar, T. J. Nonadiabatic reaction dynamics to silicon monosulfide (SiS): A key molecular building block to sulfur-rich interstellar grains. *Science Advances* **2021**, *7*, No. eabg7003.

(61) Koziar, J. C.; Cowan, D. O. Photochemical heavy-atom effects. *Acc. Chem. Res.* **1978**, *11*, 334−341.

(62) Alagia, M.; Balucani, N.; Cartechini, L.; Casavecchia, P.; van Beek, M.; Gualberto Volpi, G.; Bonnet, L.; Claude Rayez, J. Crossed beam studies of the O (^{3}P, ^{1}D)+ CH_3I reactions: Direct evidence of intersystem crossing. *Faraday Discuss.* **1999**, *113*, 133−150.

(63) Hwang, D.-Y.; Mebel, A. M. Ab initio study of spin-forbidden unimolecular decomposition of carbon dioxide. *Chem. Phys.* **2000**, *256*, 169−176.

(64) Geppert, W. D.; Naulin, C.; Costes, M. Integral cross-section of the C (^3P_J) + O_2 ($X^3\Sigma_g^-$) → CO ($X^1\Sigma^+$)+ O ($^1D_2$) reaction between 0.41 and 12.0 kJ/mol. *Chem. Phys. Lett.* **2002**, *364*, 121−126.

(65) Guo, Y.; Gu, X.; Kawamura, E.; Kaiser, R. I. Design of a modular and versatile interlock system for ultrahigh vacuum machines: A crossed molecular beam setup as a case study. *Rev. Sci. Instrum.* **2006**, *77*, 034701−034709.

(66) Kaiser, R. I.; Maksyutenko, P.; Ennis, C.; Zhang, F.; Gu, X.; Krishtal, S. P.; Mebel, A. M.; Kostko, O.; Ahmed, M. Untangling the chemical evolution of Titan's atmosphere and surface−from homogeneous to heterogeneous chemistry. *Faraday Discuss.* **2010**, *147*, 429−478.

(67) Daly, N. Scintillation type mass spectrometer ion detector. *Rev. Sci. Instrum.* **1960**, *31*, 264−267.

(68) Vernon, M. F. *Molecular beam scattering*; University of California: Berkeley, CA, 1983.

(69) Weiss, P. S. Reaction Dynamics of Electronically Excited Alkali Atoms with Simple Molecules. Ph.D. Dissertation, University of California, 1986.

(70) Schmidt, M. W.; Baldridge, K. K.; Boatz, J. A.; Elbert, S. T.; Gordon, M. S.; Jensen, J. H.; Koseki, S.; Matsunaga, N.; Nguyen, K. A.; Su, S. General atomic and molecular electronic structure system. *J. Comput. Chem.* **1993**, *14*, 1347−1363.

(71) Werner, H.-J.; Knowles, P. J.; Knizia, G.; Manby, F. R.; Schütz, M.; Celani, P.; Györffy, W.; Kats, D.; Korona, T.; Lindh, R.; et al. *A Package of Ab Initio Programs, MOLPRO*, version 2015.1; University of Cardiff: Cardiff, UK, 2015. http://www.molpro.net.

(72) Kohn, W.; Sham, L. J. Self-consistent equations including exchange and correlation effects. *Physical review* **1965**, *140*, A1133.

(73) Zhao, Y.; Truhlar, D. G. The M06 suite of density functionals for main group thermochemistry, thermochemical kinetics, non-covalent interactions, excited states, and transition elements: two new functionals and systematic testing of four M06-class functionals and 12 other functionals. *Theor. Chem. Acc.* **2008**, *120*, 215−241.

(74) Dunning, T. H., Jr Gaussian basis sets for use in correlated molecular calculations. I. The atoms boron through neon and hydrogen. *J. Chem. Phys.* **1989**, *90*, 1007−1023.

(75) Kendall, R. A.; Dunning, T. H., Jr; Harrison, R. J. Electron affinities of the first-row atoms revisited. Systematic basis sets and wave functions. *J. Chem. Phys.* **1992**, *96*, 6796−6806.

(76) Peverati, R.; Truhlar, D. G. M11-L: A local density functional that provides improved accuracy for electronic structure calculations in chemistry and physics. *J. Phys. Chem. Lett.* **2012**, *3*, 117−124.

(77) Harvey, J. N.; Aschi, M. Spin-forbidden dehydrogenation of methoxy cation: a statistical view. *Phys. Chem. Chem. Phys.* **1999**, *1*, 5555−5563.

(78) Koga, N.; Morokuma, K. Determination of the lowest energy point on the crossing seam between two potential surfaces using the energy gradient. *Chem. Phys. Lett.* **1985**, *119*, 371−374.

(79) Nunes, C. M.; Viegas, L. P.; Wood, S. A.; Roque, J. P.; McMahon, R. J.; Fausto, R. Heavy-Atom Tunneling Through Crossing Potential Energy Surfaces: Cyclization of a Triplet 2-Formylarylnitrene to a Singlet 2, 1-Benzisoxazole. *Angew. Chem., Int. Ed.* **2020**, *59*, 17622−17627.

(80) Gannon, K. L.; Blitz, M. A.; Liang, C.-H.; Pilling, M. J.; Seakins, P. W.; Glowacki, D. R.; Harvey, J. N. An experimental and theoretical investigation of the competition between chemical reaction and relaxation for the reactions of 1 CH 2 with acetylene and ethene: implications for the chemistry of the giant planets. *Faraday Discuss.* **2010**, *147*, 173−188.

(81) Knizia, G.; Adler, T. B.; Werner, H.-J. Simplified CCSD (T)-F12 methods: Theory and benchmarks. *J. Chem. Phys.* **2009**, *130*, 054104−054124.

(82) Adler, T. B.; Knizia, G.; Werner, H.-J. A simple and efficient CCSD (T)-F12 approximation. *J. Chem. Phys.* **2007**, *127*, 221106−221110.

(83) Zhang, J.; Valeev, E. F. Prediction of reaction barriers and thermochemical properties with explicitly correlated coupled-cluster methods: A basis set assessment. *J. Chem. Theory Comput.* **2012**, *8*, 3175−3186.

(84) Berning, A.; Schweizer, M.; Werner, H.-J.; Knowles, P. J.; Palmieri, P. Spin-orbit matrix elements for internally contracted multireference configuration interaction wavefunctions. *Mol. Phys.* **2000**, *98*, 1823−1833.